Screen printing of upconversion $NaYF_4$:Yb^{3+}/Eu^{3+} with Li^+ doped for anti-counterfeiting application

Dongdong Li (李冬冬)[1,†], Jianye Mo (磨建业)[1,†], Chong Wang (王 翀)[1], Wei Liu (刘 薇)[1], Haibo Ge (葛海波)[1], Dongdong Han (韩冬冬)[1], Aihua Hao (郝爱花)[1], Baoyu Chai (柴宝玉)[1], and Jiangbo She (佘江波)[2,*]

[1]*School of Electronic Engineering, Xi'an University of Post & Telecommunications, Xi'an 710121, China*
[2]*State Key Laboratory of Transient Optics and Photonics, Xi'an Institute of Optics and Precision Mechanics, Chinese Academy of Sciences, Xi'an 710119, China*
**Corresponding author: shejb@opt.ac.cn*

Received June 3, 2020; accepted July 7, 2020; posted online September 24, 2020

Li ions affect the upconversion efficiency by changing the local crystal field of the luminescent center. Herein, in order to improve the upconversion efficiency of $NaYF_4$:Yb^{3+}/Eu^{3+}, a series of $NaYF_4$:Yb^{3+}/Eu^{3+} micro-particles with different Li^+ doping concentrations were synthesized by the hydrothermal synthesis method, respectively. Firstly, the structure and morphology of $NaYF_4$:Yb^{3+}/Eu^{3+} upconversion micro-particles (UCMPs) with different doping concentrations were analyzed by X-ray diffraction and a scanning electron microscope (SEM). SEM results show that the UCMPs are not only highly crystallized, but also have hexagons with different Li^+ concentrations of $NaYF_4$:Yb^{3+}/Eu^{3+}. X-ray diffraction shows that the crystal field around Eu^{3+} changes with the increase of Li^+ concentration. Then, the fluorescence spectrum of $NaYF_4$:Yb^{3+}/Eu^{3+} was studied under the irradiation of a 980 nm laser. The results show that the fluorescence intensity of $NaYF_4$:Yb^{3+}/Eu^{3+} with 2% Li^+ is the strongest, which is twice the intensity of $NaYF_4$:Yb^{3+}/Eu^{3+} without Li^+. Finally, the fluorescence imaging analysis of $NaYF_4$:Yb^{3+}/Eu^{3+} with 2% Li^+ concentration was carried out. The UCMPs are used to screen printing to evaluate the imaging effect on different sample surfaces. The results show $NaYF_4$:Yb^{3+}/Eu^{3+} (with 2% Li^+) has great application prospects in anti-counterfeiting recognition.

Keywords: upconversion micro-particles; hydrothermal synthesis; anti-counterfeiting identification; screen printing.
doi: 10.3788/COL202018.110501.

In recent years, rare earth upconversion materials have been widely used in communication, solid-state lasers, display panels, biomedicine, and many other aspects[1–4]. Lanthanide-doped $NaYF_4$ upconversion luminescent nanophosphors have attracted great interest for anti-counterfeiting applications. In order to improve the upconversion efficiency of nanocrystals, the upconversion efficiency is improved by means of ion doping, surface modification, and lattice structure adjustment[5–8]. Upconversion materials could be applied for anti-counterfeiting fields because of their high concealment and high upconversion fluorescence efficiency[9].

Co-doped metal ions can improve the upconversion efficiency by changing the crystal field around the luminescent ions and modifying the surface of nanocrystals[10–13]. Matrix materials, sensitizers, and activators are the main factors affecting the luminescent properties of rare-earth-doped fluoride nanomaterial. Rare earth ions have a long lifetime in fluoride, forming more metastable energy levels and producing abundant energy level transitions[14]. The absorption and emission spectra of trivalent rare earth ions originate from the transitions between different energy levels of 4f electrons in the inner layer. For Eu^{3+} ions, which are widely studied and applied, it is easy to realize the fluorescence emission corresponding to $^5D_0 \rightarrow {}^7F_1$ magnetic dipole transition and $^5D_0 \rightarrow {}^7F_1$ electric dipole transition under excitation[15–17]. In comparison with oxyfluoride candidates, $NaYF_4$:Yb^{3+}/Eu^{3+} exhibits good thermal stability and high-frequency conversion efficiency[18].

Li^+ ions have many advantages, which are often used in the preparation of nanomaterials[19–21]. When preparing Li^+-doped upconversion micro-particles (UCMPs), Li^+ ions will replace the position of Na^+ ions due to their smaller radius. So, both $NaYF_4$ and $LiYF_4$ exist in the nanomaterials. The incorporation of Li^+ ions changes the symmetry of nanocrystals and improves the upconversion efficiency[22,23].

In this work, a series of $NaYF_4$:Yb^{3+}/Eu^{3+} UCMPs with different Li^+ doping concentrations were successfully prepared by the hydrothermal synthesis method. The structure, morphology, and luminescent intensity of $NaYF_4$:Yb^{3+}/Eu^{3+} UCMPs were characterized. Finally, the fluorescence imaging analysis of $NaYF_4$:Yb^{3+}/Eu^{3+} with 2% Li^+ doping concentration was carried out. The imaging results are clear and can be applied to screen printing, which shows great application prospects in anti-counterfeiting recognition.

$Li_xNa_{1-x}YF_4$:18%Yb^{3+}, 2%Eu^{3+} UCMPs were prepared by hydrothermal synthesis. Firstly, 10 mmol sodium citrate was dissolved in 10 mL deionized water in a beaker. Then, 4 mmol $Y(NO_3)_3 \cdot 6H_2O$, 0.9 mmol $Yb(NO_3)_3$, and 0.1 mmol $Eu(NO_3)_3$ were added to the beaker and magnetically stirred for 10 min to form

emulsion. Then, the 14.4 mmol NaCl or $LiNO_3$ mixture, oleic acid 10 mL, ethylene glycol 25 mL, and 30 mmol NH_4F were added in sequence according to the percentage. After stirring for 30 min, the mixture was transferred into an autoclave, sealed, and stored at 180°C for 6 h. Finally, the product was centrifuged and washed with deionized water and ethanol three times, respectively. All of the samples were dried at 80°C for 6 h before further characterization and application.

The X-ray diffraction (XRD) patterns of the samples were recorded by the Bruker D2PHASER type X-ray diffractometer using Cu Kα radiation (λ is 0.1546 nm). The size and morphology were investigated by a scanning electron microscope (SEM, KYKY 1000B). A power-adjustable laser diode (980 nm, 0 to 2 W) with a lens making the beam parallel was employed as a pump light source. The luminescence spectra were recorded by a Hitachi F-4500 fluorescence spectrophotometer [1.0 nm for spectral resolution (FWHM) of the spectrophotometer and 400 V for the photomultiplier tube (PMT) voltage] at room temperature. The camera is a high-performance CCD camera produced by Andorra, UK. The experiment was carried out at room temperature in a dark room.

The purity and morphology of $NaYF_4$:18%Yb^{3+}, 2%Eu^{3+} UCMPs with different Li^+ doping concentrations were characterized by XRD and SEM. The XRD results are shown in Fig. 1. The main diffraction peaks are 100, 110, 101, 200, 111, 201, 210, 002, 300, 211, 102, 112, 220, 311, 312, and 302. Compared with a powder diffraction file (PDF) standard card (PDF: 28-1192), there are no other miscellaneous peaks, indicating that pure UCMPs were prepared.

Figure 2 shows the diffraction peak of the nanocrystal around 43.472°. From the local magnification of the XRD images, it is found that the diffraction peak shifts to the right with the increase of Li^+ concentration. When the Li^+ doping concentration is 2% of the matrix material, the diffraction peak of the nanocrystal starts to move to the left again. The variation of the diffraction peak

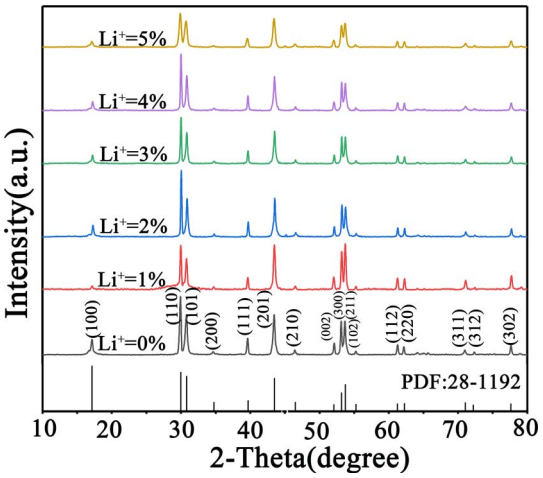

Fig. 1. XRD diffraction pattern of Li^+-doped $NaYF_4$:18%Yb^{3+}, 2%Eu^{3+}.

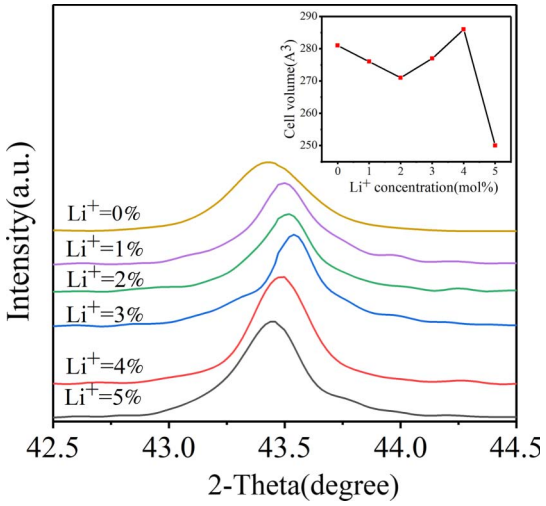

Fig. 2. Diffraction peak of Li^+-doped $NaYF_4$:18%Yb^{3+}, 2% Eu^{3+} UCMPs around 43.472°.

of $Li_xNa_{1-x}YF_4$:18%Yb^{3+}, 2%Eu^{3+} phosphor is nonlinear with the concentration of Li^+ impurity, which is due to the lattice shrinkage at low concentration and the lattice expansion again after reaching a certain concentration[24]. The radii of the Li^+ ion and Na^+ ion are 0.68 Å and 0.97 Å (1 Å = 0.1 nm), respectively. The radius of the Li^+ ion is smaller than that of metal Na^+ ion. When metal Li^+ ions are doped into the nanocrystal, Li^+ ions will replace the position of the Na^+ ion and fill the gap position at the same time. The lattice will shrink and then change the lattice symmetry, which can improve the up conversion efficiency of the nanocrystal.

From Bragg's law,

$$2d\sin\theta = n\lambda.$$

In the formula, d is the distance between planes, θ is the diffraction angle, and λ is the diffraction wavelength. When a certain amount of Li^+ ions are added into the gap, a large number of Li^+ ions will pour into the gap, which will lead to the increase of the inter planar distance, the decrease of the diffraction angle θ, and the expansion of $Li_xNa_{1-x}YF_4$:18%Yb^{3+}, 2%Eu^{3+} lattice. As a result, the diffraction peak around 43.472° moves first to the right and then to the left.

As shown in Fig. 3, the $NaYF_4$:18%Yb^{3+}, 2%Eu^{3+} with different Li^+ doping concentrations is tested by SEM. In Figs. 3(a)–3(f), the Li^+ impurity concentrations are 0%, 1%, 2%, 3%, 4%, and 5%, respectively. Since the Li^+ ions with different concentrations have little effect on the particles size, the size of micro-crystals is about 180 nm, and the shape is a hexahedron with different Li^+ ions doping concentrations. It was found that the morphology has no change with the further increase of metal ion concentration, and the size has no obvious change[25].

The energy level transition diagram of Li^+-doped $Li_xNa_{1-x}YF_4$:18%Yb^{3+}, 2%Eu^{3+} is shown in Fig. 4 under

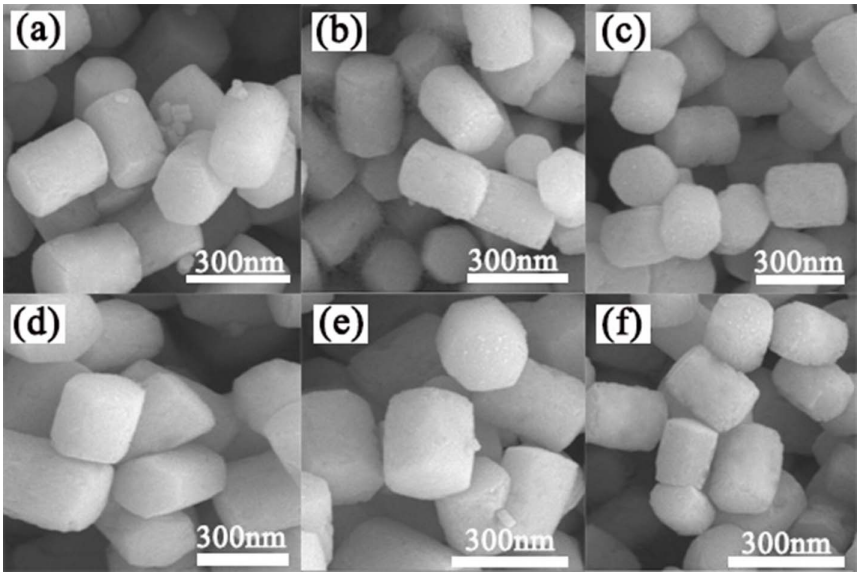

Fig. 3. SEM images of Li^+-doped $NaYF_4$:18%Yb^{3+}, 2%Eu^{3+}.

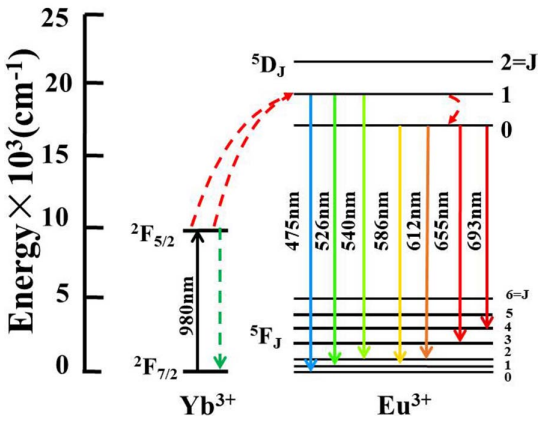

Fig. 4. Schematic diagram of energy level transition of Li^+-doped $NaYF_4$:18%Yb^{3+}, 2%Eu^{3+}.

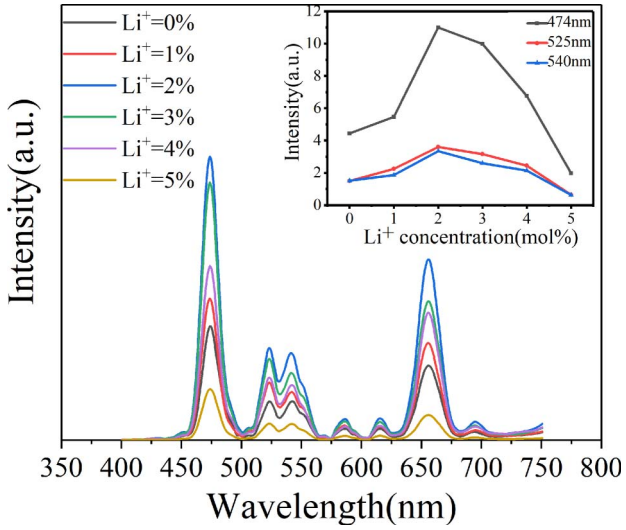

Fig. 5. Fluorescence spectra of $Li_xNa_{1-x}YF_4$:18%Yb^{3+}, 2%Eu^{3+} with different Li ion doping concentrations.

the irradiation of 980 nm lasers. After the Yb^{3+} ion absorbs laser energy, the two photon absorption occurs. The excited unstable electrons transfer energy to the activator Eu^{3+} ion by cross relaxation forming excited-state $^5D_1$ level. The emission spectra of Eu complexes display seven peaks in the 475–655 nm region associated with the $^5D_J \rightarrow {}^7F_J$ transitions of the Eu^{3+} ion (Fig. 5).

The fluorescence spectra of $Li_xNa_{1-x}YF_4$:18%Yb^{3+}, 2%Eu^{3+} with 0%, 1%, 2%, 3%, 4%, and 5% Li^+ ions were examined, respectively. Figure 5 shows the fluorescence spectra of $Li_xNa_{1-x}YF_4$:18%Yb^{3+}, 2%Eu^{3+} doped with different Li ions under 980 laser excitation. The luminescence intensity increases continuously with the Li doping concentration change from 0% to 2%; then the intensity decreases with the addition of more Li ions. Among these samples, the luminescence intensity reaches the maximum value with 2% Li^+ doping concentration. Hence, the optimal Li^+ doping concentration is 2%.

Furthermore, based on the upconversion fluorescence spectra, we further evaluated molecular pixel behavior of red, green, blue (RGB) $Li_xNa_{1-x}YF_4$:18%Yb^{3+}, 2%Eu^{3+} by reproducing colors in the International Commission on Illumination (CIE) 1931 *XYZ* color space and the *xy* chromaticity diagram. The CIE of the $Li_xNa_{1-x}YF_4$:18%Yb^{3+}, 2%Eu^{3+} sample is shown in Fig. 6. The visible light colors of the UCMPs are marked in the CIE color coordinates. The chromaticity coordinates (x, y) of RGB UCMPs in solution were (299,0,10) for UCMPs-R, (140,253,4) for UCMPs-G, and (2,150,252) for UCMPs-B.

Due to their high concealment and high upconversion fluorescence efficiency, upconversion luminescent materials can be applied to fingerprint identification. In this experiment, $Li_xNa_{1-x}YF_4$:18%Yb^{3+}, 2%Eu^{3+} with 2% Li^+

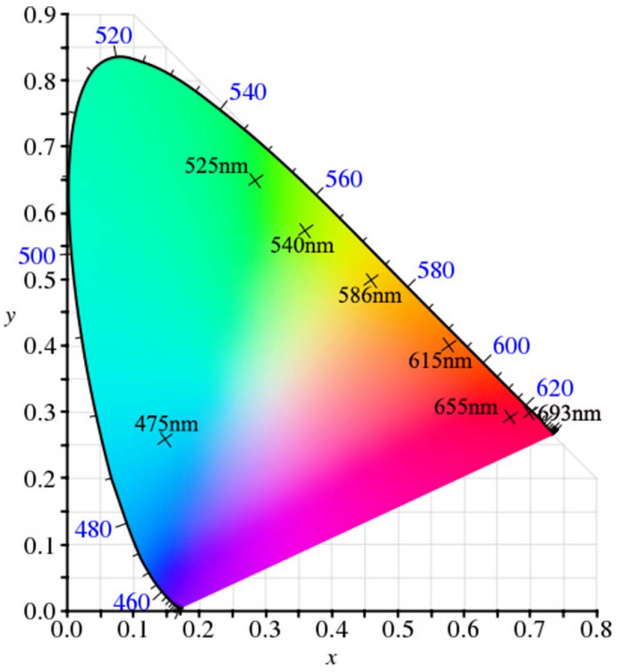

Fig. 6. CIE of Li^+-doped $NaYF_4$:18%Yb^{3+}, 2%Eu^{3+}.

was applied to screen printing. The screen printing process is shown in Fig. 7. The screen printing plate was purchased. Firstly, UCMPs were mixed with ethanol to make the upconversion micro-printing agent. Then, the screen printing agent was evenly coated on the plate, the brush was used up and down, and the printing agent was evenly covered with the pattern as far as possible during the brushing process. Then, the printing template was used to print the pattern to the surface of the printing table so that the printed sample is prepared and dried at room temperature. The sample was placed in a dark environment and exposed to 980 nm of laser for imaging experiments. The CCD camera was used to photograph the printed pattern clearly.

Screen printings were made on various materials in daily life: a plastic sheet, compact disk, glass sheet, and metal cover. The results of the imaging experiments are shown in Fig. 8. From the top to the bottom, the first row images are taken before printing. The middle row pictures are the patterns under the laser irradiation of 980 nm in the strong light environment, and the last row pictures are taken under the laser irradiation of 980 nm in the dark room environment. All of the print patterns can be seen in the dark room. But, in the strong light environment, the print patterns on the plastic sheet and compact disk are indistinct. On the glass sheet and metal cover the print pattern appeared almost the same in strong light and dark environment, which can be applied to anti-counterfeiting identification.

In summary, a series of $NaYF_4$:Yb^{3+}/Eu^{3+} UCMPs with different concentrations of Li ion doping were synthesized by the hydrothermal synthesis method. Different Li ion doping concentrations will change the crystal field around Eu^{3+} ions and break the symmetry of the lattice structure. The results show that the $NaYF_4$:Yb^{3+}/Eu^{3+} doped with different concentrations of Li ions has good crystallinity. The emission peaks of Eu^{3+} ions are 475 nm, 525 nm, 540 nm, 586 nm, 615 nm, and 655 nm under the excitation of the 980 nm laser by fluorescence spectrum analysis when different concentrations of Li ions are incorporated. With the increase of incorporation of Li^+, the luminescence intensity is gradually enhanced firstly and then gradually weakened. This is because more cubic phase of $Li_xNa_{1-x}YF_4$:18%Yb^{3+}, 2%Eu^{3+} is converted into hexagonal phase, and the luminescence efficiency is improved. With the increase of Li^+ doping concentration, the grain size decreases, which leads to the increase of surface quenching points, the enhancement of the non-radiation energy transfer process, and the decrease of luminescence efficiency[26]. The luminescence intensity reaches the strongest when the doping concentration of Li ions is 2%. Finally, the synthesized $NaYF_4$:Yb^{3+}/Eu^{3+}

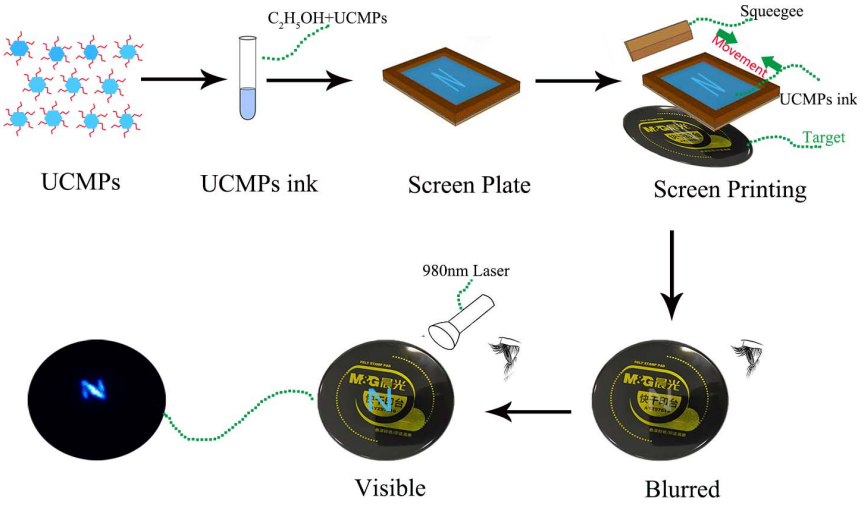

Fig. 7. Screen printing imaging process.

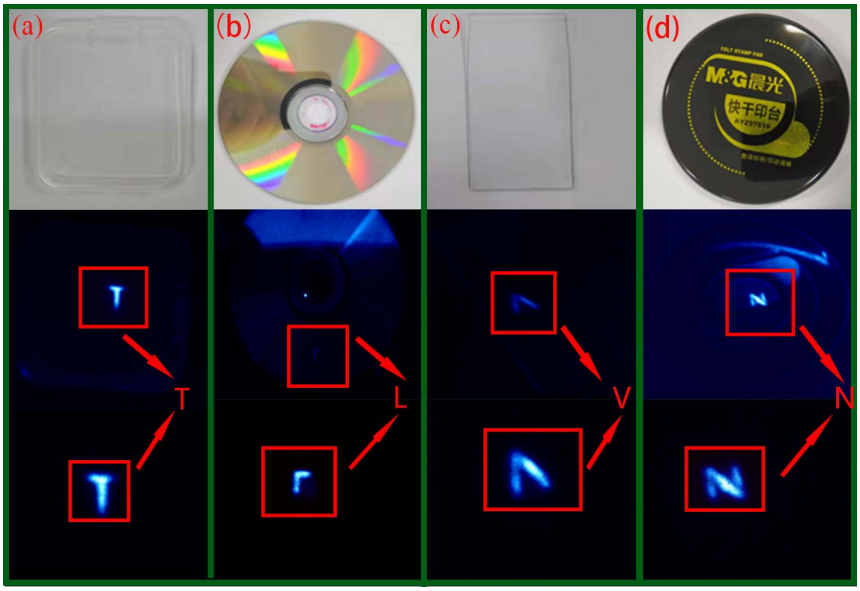

Fig. 8. Screen printing imaging results of different materials. (a) Plastic, (b) optical disc, (c) glass, (d) printing table.

UCMPs were made into a screen printing agent. Different characters were printed on different materials using the engraved screen printing template. The printed pattern is clearly visible under the laser irradiation of 980 nm. The prepared $Li_xNa_{1-x}YF_4$:18%Yb^{3+}, 2%Eu^{3+} has potential application prospects in anti-counterfeiting recognition.

This work was supported by the National Natural Science Foundation of China (No. 61805198) and the Special Research Projects of Department of Education of Shaanxi Province (No. 18JK0707).

†These authors contributed equally to this work.

References

1. N. Li, H. H. Tan, S. W. Xie, S. M. Liu, C. Tong, M. Ouyang, and L. Xu, J. Nanosci. Nanotechnol. **20**, 1866 (2020).
2. L. M. Wiesholler, C. Genslein, A. Schroter, and T. Hirsch, Anal. Chem. **90**, 14247 (2018).
3. J. X. Tang, D. G. Yin, X. Y. Zhang, L. Zhang, Y. Liu, T. Zhang, and N. Chang, J. Nanosci. Nanotechnol. **17**, 1393 (2017).
4. X. Liu, R. S. Lei, F. F. Huang, D. G. Deng, H. P. Wang, S. L. Zhao, and S. Q. Xu, Chin. Opt. Lett. **17**, 111601 (2019).
5. P. Xiao, S. Ye, H. Z. Liao, and D. P. Wang, J. Alloys Compd. **767**, 775 (2018).
6. X. K. Xu, W. Li, W. Zhou, G. Tan, Y. Zheng, C. Hu, B. Lei, X. Zhang, Y. Liu, and J. Zhuang, J. Mater. Chem. C **6**, 10360 (2018).
7. A. A. Lyapin, S. V. Gushchin, A. S. Ermakov, S. V. Kuznetsov, P. A. Ryabochkina, V. Y. Proydakova, V. V. Voronov, P. P. Fedorov, and M. V. Chernov, Chin. Opt. Lett. **16**, 091901 (2018).
8. F. T. Rabouw, P. T. Prins, P. Villanueva-Delgado, M. Castelijns, R. G. Geitenbeek, and A. Meijerink, Am. Chem. Soc. **15**, 4812 (2018).
9. W. Yao, Q. Tian, J. Liu, Z. Wu, S. Cui, J. Ding, Z. Dai, and W. Wu, J. Mater. Chem. C **26**, 6327 (2016).
10. L. Li, K. Green, H. Hallen, and S. F. Lim, Nanotechnology **26**, 025101 (2014).
11. B. Shao, Z. W. Yang, Y. D. Wang, J. Li, J. Yang, J. Qiu, and Z. Song, ACS Appl. Mater. Interf. **7**, 2 (2015).
12. Y. L. Wang, F. Nan, Z. Q. Cheng, J. Han, Z. Hao, H. Xu, and Q. Wang, Nano Res. **8**, 2970 (2015).
13. S. Li, Y. Song, X. Chen, T. Liu, Z. Guo, and D. Wang, J. Rare Earths **35**, 753 (2017).
14. M.Q. Yu, Y. Qu, K. Pan, G. Wang, and Y. Li, Sci. China Mater. **60**, 228 (2017).
15. J. F. Yang, L. N. Song, X. X. Wang, J. Dong, S. Gan, and L. Zou, Dalton Trans. **47**, 1294 (2018).
16. S. H. Zhang, S. Z. Chen, C. Y. Gao, Y. Jin, G. Jia, Z. Li, D. Liu, X. Liang, X. Yang, and J. Zhang, Sci. China **60**, 130 (2017).
17. J. D. Wang, Q. Zhen, M. Hojamberdiev, S. Zheng, and Y. Xu, J. Rare Earths **36**, 353 (2018).
18. P. Cai, X. Wang, and H. J. Seo, Phys. Chem. Chem. Phys. **20**, 2028 (2018).
19. V. Preeti, S. Debasish, and R. Parasmani, Crystal Growth Design **20**, 468 (2019).
20. H. Lin, D. Xu, D. D. Teng, S. Yang, and Y. Zhang, Opt. Mater. **45**, 229 (2015).
21. D. W. Wang, S. H. Huang, F. T. You, S. Qi, Y. Fu, G. Zhang, J. Xu, and Y. Huang, J. Luminescence **122**, 450 (2007).
22. C. Z. Zhao, X. G. Kong, X. M. Liu, L. P. Tu, F. Wu, Y. L. Zhang, K. Liu, Q. H. Zeng, and H. Zhang, Nanoscale **5**, 8084 (2013).
23. S. Som, C.-Y. Yanga, C.-H. Lu, and S. Das, Ceramics Int. **45**, 5703 (2019).
24. A. K. Singh and S. K. Singh, RSC Adv. **4**, 27039 (2014).
25. X. Wang, W. Ye, J. Yu, Y. Bu, and X. Yan, Opt. Express **26**, 21950 (2018).
26. X. W. Wang, X. Zheng, Y. B. Wang, H. Li, J. Xie, T. Wei, Q. Huang, X. Xie, L. Huang, and W. Huang, Dalton Trans. **46**, 8968 (2017).